15TH IEA HEAT PUMP CONFERENCE
MAY 26–29, 2026 | HOFBURG
VIENNA 2026
DECARBONISATION THROUGH INNOVATION

Bi-level Optimization of the Configuration and Operation of Solar Energy Heat Pumps

Kaixuan Hu [a], Rui Xu [a], Fang Liu [a, b, *]

[a] College of Energy and Mechanical Engineering, Shanghai University of Electric Power, Shanghai, 200090, China
[b] Shanghai Non-Carbon Energy Conversion and Utilization Institute, Shanghai, 200240, China

Abstract

In the context of China's dual carbon goals, efficient energy utilization is a critical issue. Given that buildings consume significant amounts of heating and cooling energy, this paper constructs a microgrid that solely uses renewable energy for power generation/heating, with the heat pump providing both heating and cooling loads, and only exchanges electricity with the regional grid. Through a two-level optimization approach, this paper considers both the economic and environmental aspects of microgrid operation. Additionally, we incorporate electricity demand response through an elasticity matrix, which can reduce thermal loads and improve user comfort. The results show that when demand response is taken into account in the microgrid, the optimized heat pump capacity is 27.73 kW and the configured area of PV/T is 252.08 m², with the latter increasing by 17.75%. In this case, the microgrid utilizes more renewable energy such as solar direct heating, with its utilization volume rising by 20.19%. Additionally, the peak shaving and valley filling coefficient is increased by 25.15% after demand response, and the system's typical daily electricity price decreases by 42.67%.

Keywords: PV/T; CO2 ejector heat pump; microgrid; bi-level optimization; demand respond

Glossary			
SEHP	Solar ejector heat pump	$C_{cap,i}$	The rated capacity of equipment i(kW or kWh)
CHHP	Cold and hot dual supply heat pump	Δt	Length of the operation time period(h)
COP	Coefficient of performance	C_{inv}	Annualized investment cost(yuan)
Q	Heat power (kJ)	k	Annual interest rate(yuan)
P	Electricity power (kWh)	y	Capital recovery period(year)
η	efficiency	C_m	System maintenance cost(yuan)
Bat	battery	$C_{om,i}$	Maintenance coefficient per unit energy of equipment i(yuan/kW or yuan/kWh)
Pv	Photovoltaic efficiency	$P_{i,t}$	The output power of equipment i during time period t(kW)
G	Global solar radiation (W/m^2)	C	Price(yuan)
η_e	Photovoltaic efficiency (-)	P	Power(kW)
f_{act}	Fraction of photovoltaic surface activity	P_L^2	Peak-shaving and valley-filling coefficient(-)
A_{pv}	effective area of the photovoltaic panel (m^2)	T	The end time of operation;Total operating time(h)
$\eta_{DC/AC}$	Inverter efficiency (-)	$P_{net,t}^{e}$	The power consumed in the microgrid at time t(kWh)
P_t	Local wind speed corresponding to generator power(m/s)	$P_{net,av}^{e}$	The average power consumed by the microgrid at each moment within an operating cycle(kWh)
$scale$	Scale parameters of the wind turbine(-)	Q	Heat(kJ)
h	The height of the wind wheel above the ground in wind power generation equipment(m)	Superscript/ Subscript	
h_{ref}	Unit reference height(m)	Pcm	Pcm thermal storage tank
y	Unit height index(-)	ch	charge
$V_{ref,t}$	Reference wind speed of the meteorological station(-)	dis	discharge
E	Power price(yuan/kWh)	Max	maximum
E_a	Self-elasticity coefficient(-)	min	minimum
E_b	Cross-elasticity coefficient(-)	t	Time t
a/p/b	Parameters of electricity price elasticity curve(-)	t+1	Time t+1

* Corresponding author.
E-mail address: fangliu@shiep.edu.cn (Fang Liu)

15th IEA Heat Pump Conference 2026 - NAI4.2 - https://doi.org/10.23697/y6vg-vx43

P_{load}	Users' non-heating electric load(kWh)	Δt	Length of time period
W	The proportion of this type of electrical load in users' non-heating electric load(-)	f	Peak period
F_j	Electric price after demand response at moment j(yuan/kWh)	p	Usual period
F_j^0	The original electric price at moment j(yuan/kWh)	g	Valley period
ϕ_t^{PMV}	The predicted average evaluation of predicted mean vote	SL	Transferable electric load
T_c	Human body surface skin temperature(°C)	CL	Reducible electric load
T_t^{in}	The indoor environmental temperature of the building at time t(°C)	min	Minimum
Me	Human body metabolic rate(%)	max	Maximum
T^{in}	Standard heating environmental temperature(°C)	in	Flow into this microgrid
$k_{down/up}$	The lower/upper limit of the heating supply elasticity coefficient(-)	out	Flow from this microgrid
C_{CO_2}	Carbon trading price(yuan)	grid	Regional power grid
α_{gr}	Basic carbon trading price(yuan)	pv	Photovoltaic panel
ST_β	The number of carbon trading tiers(yuan)	wt	Wind turbine
α_{ad}	The proportion of the increased price of carbon trading in each tier to the basic carbon trading price(-)	t	At time t
TR_{CO_2}	Electricity-carbon conversion coefficient(-)	tot	All power supplements
CRF_i	The capital recovery factor of equipment i(-)	hp	Heat pump
$C_{unit,i}$	Unit investment cost of equipment i(yuan/kW or yuan/kWh)	pcm	Water and pcm two stage thermal storage
$P^{re}(t)$	power of on-site consumption of new energy(kWh)	eqL	Equal

1.Introduction

Microgrids, which include distributed generation, user-side loads, and energy storage, are considered the foundation for future smart energy development [1]. Under the dual carbon goals, heat pumps are seen as having significant potential for carbon neutrality[12], leading to their widespread application in current microgrid research. Bahman et al. [3] proposed a combined cooling and power supply system using water-source heat pumps for industrial users. Li et al. [5] developed an energy system model for data centers using CO2 heat pumps and compressed CO2 storage to study its operational optimization scheduling. Qi et al. [2] used ground-source heat pumps in microgrids, considering the impact of seasonal thermal balance on the COP and lifespan of heat pumps. Zhang et al.[6] utilized a ground-source heat pump system, reducing the cost of the system. Regarding the conversion of heat pumps to electric heating, solar heat pumps (especially those using PV/T) can use renewable energy to improve the system's electric-to-thermal conversion efficiency. For example, Mi et al. [4] considered typical daily meteorological conditions and influent and effluent water temperatures to study the optimized scheduling of solar photovoltaic thermal heat pumps for hot water supply. However, current research still focuses on the application of solar heat pumps in microgrids.

Due to the current increase in renewable energy power plants, demand response, as an important load-side flexibility resource, can help balance the grid peak and off-peak loads[7]. Flexibility is a crucial evaluation criterion for demand response; the higher the system flexibility, the faster it can return to normal operation after a disaster[8]. Using flexibility resources in the system also enhances grid flexibility. Traditional grid flexibility is usually achieved through adjustments from source-side resources. Regarding the comparison of grid-side, load-side, and storage-side resource flexibility, relevant studies[9] show that the flexibility potential of electric boilers exceeds that of wet electrical appliances, and significant load fluctuations during the day lead to partial curtailment of solar power. Wang et al.[10] proposed an optimization scheduling model based on opportunity constrained programming (CCP) to coordinate multiple energy sources and improve microgrid flexibility. Yang et al.[11] established a stochastic coordinated generation and transmission expansion planning model considering the impact of demand response schemes for research purposes. Lin et al.[13]considered the cascaded coupling of thermal energy, dividing user heat loads and heat sources into high and low temperature levels to build the basic framework of a low-carbon district heating system, better matching thermal supply and demand in terms of quality. They also developed a mathematical model for electricity and heat planning loads considering integrated electric-thermal demand response, evaluating the framework in three stages. For the research of power demand response, some scholars have also introduced the predicted demand baseline. For example, Li et al.[15] proposed a framework integrating the predicted demand baseline, BESS specification and ToU pricing to simultaneously formulate the optimal BESS deployment and small-based TOG in target buildings.

For the optimization of microgrids, Yang et al.[13] proposed a linear rainflow counting algorithm to identify ESS charge-discharge half-cycles, converting them into mixed integer linear programming (MILP) problems, thereby enabling the assessment of the cycle life of energy storage systems (ESS) during the optimization process. Kang et al.[22]constructed a dual-layer collaborative optimization model to optimize equipment capacity and operational strategies separately, using genetic algorithms and mixed integer linear programming for solving, thereby enhancing system performance and efficiency. Kirchem et al.[18] studied the potential of wastewater treatment plants (WWTPs) in Ireland to achieve demand response (DR) through aeration and wastewater pumping processes, analyzing its impact on the power system, including costs, emissions, and renewable energy integration. The study focused on the role of WWTPs in load balancing in the power system and how to optimize energy consumption while meeting wastewater treatment process constraints. Dual-layer optimization can simultaneously seek the optimal configuration and operational strategy for microgrids.

In current scholarly research, the establishment of microgrid models often takes a large park as its foundation, incorporating both power and heat grids. Boilers are typically added to supplement heating or power supply, achieving multi-source complementarity. However, urban buildings in southern China often lack connections to heat grids and are constrained by site conditions, with most thermal loads being converted from electrical energy.

This paper establishes a thermally isolated microgrid. To simulate the typical building microgrid in non-heating areas of China, the microgrid established in this paper relies solely on heat pumps for cooling and heating conversion. A dual-layer optimization method of capacity-operation is adopted to optimize the configuration within the microgrid and derive the optimal operating strategy. On this basis, considering demand response, the peak-to-valley difference of time-of-use electricity prices after increasing the typical daily demand response is utilized to achieve peak shaving and valley filling through price-based demand response. The base carbon price is sourced from the Chinese carbon trading platform, and a tiered carbon trading system is used to increase the proportion of renewable energy in the microgrid's energy mix. This paper provides recommendations for the configuration and operation strategies of existing boiler-free buildings in cities. The contributions of this paper are:

1. A thermal isolated microgrid system with only heat pump as cold and heat source is established, and the price of electricity demand response is studied, considering that user comfort setting can reduce the heat load.
2. A tiered carbon trading system is established, using capacity and operational double optimization, and comparing scenarios with and without carbon trading, it is found that considering carbon trading can help increase initial renewable energy investment.

The structure of this paper is as follows: we first establish the microgrid model (Chapter 2), and in Chapter 3. we construct the double-layer optimization model of capacity and operation. Then, we optimize the model established in this paper through a practical case of a school (Chapter 4).

2.Model building

2.1 Heat pump microgird model

As shown in Figure 1, a system incorporating a solar phase change energy storage heat pump, solar panels, fans, and photovoltaic-thermal (PV/T) modules is established. The solar panels, fan power generation, PV/T power generation, and heat production are dynamically simulated by Dymola. Both the solar heat pump thermal storage mode and the direct heating mode using the solar heat pump can supply heat directly through a centralized hot water tank.

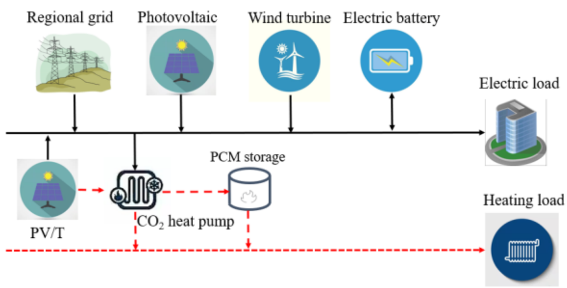

Fig. 1. Microgrid structure with solar heat pump

2.1.1 Solar phase change energy storage heat pump model

In order to simplify the calculation of this chapter, the average COP of the heat pump operating in different modes is obtained through the dynamic calculation of Dymola[32] and modeled on Matlab using the following formula.

$$Q_{hp}(t) = COP_{SEHP}(t)P_{SEHP}(t) + COP_{CHHP}(t)P_{CHHP}(t) \tag{1}$$

$$SOC_{pcm}(t+1) = SOC_{pcm}(t)(1-\delta_{pcm}) + (Q_{pcm}^{ch}(t)\eta_{pcm}^{ch} - \frac{Q_{pcm}^{dis}(t)}{\eta_{pcm}^{dis}})\Delta t \tag{2}$$

$$0 \le Q_{pcm}^{ch}(t)\eta_{pcm}^{ch} \le Q_{pcm_{max}}^{ch} \tag{3}$$

$$SOC_{pcm}^{min}(t) \le SOC_{pcm}(t) \le SOC_{pcm}^{max}(t) \tag{4}$$

Among them, hp is the heat pump, SEHP is the solar heat pump mode, and CHHP is the cold and hot dual heat pump mode. It is assumed that the former can only operate under the condition of solar radiation. pcm is the abbreviation of water multi-stage phase change heat storage tank, and SOC_{pcm} is the heat storage state of the heat storage tank (analogous to the SOC of a battery).

2.1.2 Battery model

In the system, take lead-acid battery energy storage system as an example. The battery state is described by the SOC of the battery, and the charge and discharge of the battery are limited.

$$SOC_{bat,t+1} = SOC_{bat,t}(1-\delta_{bat}) + (P_{bat,t}^{ch}\eta_{bat}^{ch} - \frac{P_{bat,t}^{dis}}{\eta_{bat}^{ch}})\Delta t \tag{8}$$

In the formula: $SOC_{bat,t}$ is the real-time capacity of the battery; δ_{bat} is the self-loss efficiency value of the battery; $P_{bat,t}^{ch}$ and $P_{bat,t}^{dis}$ are the charging and discharging power of the battery respectively; η_{bat}^{ch} and η_{bat}^{dis} are the charge and discharge efficiency of the battery respectively; $\Delta t$is the unit time interval, and the value is 1h.

2.1.3 Photovoltaic power generation model

The photovoltaic power generation model has been established in the literature[26]. The photovoltaic power generation module model is established using the Buildings model library PV Simple Oriented module, as shown in Figure 3. The power generation calculation is as follows:

$$P_{pv,t} = A_{pv} \cdot \eta_e \cdot f_{act} \cdot \eta_{DC/AC} \cdot G \tag{9}$$

2.1.4 Wind power generation model

The wind power generation model is established by using the Wind Turbine module of Buildings model library, as shown in Figure 4. The power generation calculation is as follows:

$$P_{WT}(t) = P_t \cdot \eta_{DC/AC} \cdot scale \tag{10}$$

$$P_t = \frac{1}{2} c_p \cdot \rho_a \cdot A_{wt} \cdot V_{loc,t}^3 \tag{11}$$

$$V_{loc,t} = V_{ref,t} \cdot (\frac{h}{h_{ref}})^y \tag{12}$$

In the formula: c_p is the wind energy utilization coefficient; ρ_a is the air density; A_{WT} is the swept area of the wind turbine; *scale* is the scale parameter of the wind turbine; P_t is the power generated by the generator corresponding to the local wind speed; h_{ref} is the height of the rotor above ground in wind power generation equipment; href is the reference height of the unit; y is the height index of the unit; $V_{ref,t}$ is the reference wind speed at the meteorological station.

2.2 Demand-side and external mechanism regulation model

2.2.1 Demand response model

This study uses the price-based demand response incentive model. Due to the different sensitivity of various loads to price response, the loads participating in the price-based demand response can be divided into transferable loads and reducible loads[27]. According to the Ref.[27], the sensitivity of users to power price changes can be modeled by introducing the electricity price elasticity matrix, so as to obtain the self-elasticity coefficient and cross-elasticity coefficient, and solve the quantity of this kind of load.

The electricity price elasticity matrix represents the influence of the fluctuation of electricity price on the electricity consumption of users within a certain time range, and the electricity price elasticity coefficient can be processed according to relevant methods in economics[27].

The elastic matrix based on time-sharing electricity price can be expressed as $\begin{bmatrix} E_{ff} & E_{fp} & E_{fg} \\ E_{pf} & E_{pp} & E_{pg} \\ E_{gf} & E_{gp} & E_{gg} \end{bmatrix}$, The subscripts f, p and g represent peak, flat and valley respectively, E_{ff}, E_{pp} and E_{gg} are the self-elasticity coefficients,and the remaining elements are cross elasticity coefficients. The simplified calculation formulas for the self-elasticity coefficients and cross-elasticity coefficients referenced from the relevant literature[28] are not listed here.

Reference[29], the calculation of transferable and reducible loads after demand response is shown in the following formula:

$$P_{DR_{SL}} = W_{SL} \cdot P_{load} \cdot \begin{bmatrix} 0 & E_{fp} & E_{fg} \\ E_{pf} & 0 & E_{pg} \\ E_{gf} & E_{gp} & 0 \end{bmatrix} \cdot \frac{F_j - F_j^0}{F_j^0} \tag{13}$$

$$P_{DR_{SL}} = W_{CL} \cdot P_{load} \cdot \begin{bmatrix} E_{ff} & 0 & 0 \\ 0 & E_{pp} & 0 \\ 0 & 0 & E_{gg} \end{bmatrix} \cdot \frac{F_j - F_j^0}{F_j^0} \tag{14}$$

2.2.2 Staged carbon trading model

Among them, C_{CO_2} is the carbon trading price; α_{gr} is the base carbon trading price, set at 0.1 yuan/kg[31];ST_β is the number of carbon trading tiers, which is set to three in this paper; α_{ad} is the ratio of the increase in price per tier of carbon trading relative to the base carbon trading price, assumed to be α_{ad}=0.25 in this paper;TR_{CO_2} is the electricity-to-carbon conversion coefficient, assuming that all power purchased by the microgrid is generated from fossil fuels, with TR_{CO_2}= 0.9 $kgCO_2$/kWh[33].

$$C_{CO_2} = \sum_{1}^{\beta} \alpha_{gr} \cdot \left[1 + \left(ST_\beta - 1\right) \cdot \alpha_{ad}\right] \cdot TR_{CO_2} \cdot P_{grid}^{in} \tag{15}$$

2.3 Evaluation indicators

（1）Annualized investment cost

$$C_{inv} = \sum_i CRF_i \cdot C_{unit,i} \cdot C_{cap,i} \tag{16}$$

$$CRF_i = \frac{k \cdot (1+k)^y}{(1+k)^y - 1} \tag{17}$$

（2） System maintenance costs

$$C_m = \sum_i \sum_t C_{om,i} \cdot P_{i,t} \cdot \Delta t \tag{18}$$

（3） System operating costs

$$C_{op} = \sum_t \Delta t \cdot [C_{grid}^{in}(t) \cdot P_{grid}^{in}(t) + C_{grid}^{out}(t) \cdot P_{grid}^{out}(t)] \tag{19}$$

（4） Effective penetration of renewable energy[26]

$$\varepsilon = \frac{\sum_{t=1}^{T} P^{re}(t)}{\sum_{t=1}^{T} P_{tot,t}} \tag{20}$$

（5） Peak and valley filling coefficient

$$P_L^2 = \frac{1}{T} \sum_{t=1}^{T} \left(P_{\text{net},t}^{\text{e}} - P_{\text{net,av}}^{\text{e}}\right)^2 \tag{21}$$

（6） PV/T direct heating ratio

$$\varepsilon_r = \frac{\sum_{t=1}^{T} Q_{PV/T}(t)}{\sum_{t=1}^{T}(Q_{hp}(t) + Q_{PV/T}(t))} \tag{22}$$

3 Bi-level optimization method

In this section, a bi-level optimization method is adopted to optimize the established heat pump microgrid model. The upper layer is configuration optimization, with the minimum value of initial investment cost, maintenance cost and electricity cost as the objective function, emphasizing the economy of the system. The lower layer is the minimum value of electricity cost and carbon emission cost as the objective function, emphasizing the economic and environmental protection of the system operation.

3.1 Upper model —— configuration optimization

(1) Objective function

The upper model takes the minimum annualized cost of the system as the objective function:

$$MinC_{up} = C_{inv} + C_m + C_{op} + C_{CO_2} \tag{23}$$

(2) Constraints

$$E_{bat,min} \le E_{bat} \le E_{bat,max} \tag{24}$$

$$E_{pcm,min} \le E_{pcm} \le E_{pcm,max} \tag{25}$$

$$E_{hp,min} \le E_{hp} \le E_{hp,max} \tag{26}$$

3.2 Lower layer model —— operation optimization

(1) Objective function

$$MinC_{down} = C_{op} + C_{CO_2} \tag{27}$$

(2) Constraints

The constraints are divided into electric balance constraint, thermal balance constraint, unit constraint, and power purchase and sale constraint with the external regional power grid.

1. Energy balance constraints

i Power balance constraints

$$\begin{aligned} &P_{wt}(t) + P_{pv}(t) + P_{PV/T}(t) + P_{grid}^{in}(t) + P_{bat}^{dis}(t) \\ &= P_{hp}(t) + P_{grid}^{out}(t) + P_{bat}^{ch}(t) + P_{load}(t) + P_{load_{DR}}(t) \end{aligned} \tag{28}$$

In the formula, $P_{wt}(t)$, $P_{pv}(t)$, and $P_{PV/T}(t)$ represent the power generated by the wind turbine, photovoltaic (PV) panel, and photovoltaic/thermal (PV/T) system at time t, respectively. $P_{grid}^{in}(t)$ and $P_{grid}^{out}(t)$ denote the electric energy drawn from the power grid and fed back to the power grid, respectively. $P_{hp}(t)$ is the power consumption of the heat pump. $P_{bat}^{ch}(t)$ and $P_{bat}^{dis}(t)$ are the charging and discharging powers of the battery at time t, respectively. $P_{load_{DR}}(t)$ is the electricity load modified by demand response.

ii Thermal energy balance constraints

$$\begin{aligned} &(1 - k_{down}) \sum_{t=1}^{T} Q_{eqL}(t) \\ &\le \sum_{t=1}^{T} (Q_{hp}(t) + Q_{pcm}(t) + Q_{PV/T}(t)) \le \left(1 + k_{up}\right) \sum_{t=1}^{T} Q_{eqL}(t) \end{aligned} \tag{29}$$

In the formula, $Q_{eqL}(t)$ represents the equivalent heat load at time t.

2. Unit constraints

$$P_{hp}^{min} \le P_{hp}(t) \le P_{hp}^{max} \tag{30}$$

$$P_{as}^{min} \le P_{as}(t) \le P_{as}^{max} \tag{31}$$

$$P_{grid}^{min} \le P_{grid}(t) \le P_{grid}^{max} \tag{32}$$

$$0 \le P_{bat}^{ch}(t)\eta_{bat}^{ch} \le P_{bat_{max}}^{ch} \tag{33}$$

$$0 \le \frac{P_{bat}^{dis}(t)}{\eta_{bat}^{dis}} \le P_{bat_{max}}^{dis} \tag{34}$$

$$SOC_{bat}^{min}(t) \le SOC_{bat}(t) \le SOC_{bat}^{max}(t) \tag{35}$$

$$P_{bat}(t) = P_{bat}^{ch}(t) - P_{bat}^{dis}(t) \tag{36}$$

$$Q_{hp}(t) = COP_{SEHP}(t)P_{SEHP}(t) + COP_{CHHP}(t)P_{CHHP}(t) \tag{37}$$

$$SOC_{pcm}(t+1) = SOC_{pcm}(t)(1-\delta_{pcm}) + (Q_{pcm}^{ch}(t)\eta_{pcm}^{ch} - \frac{Q_{pcm}^{dis}(t)}{\eta_{pcm}^{dis}})\Delta t \tag{38}$$

$$0 \le Q_{pcm}^{ch}(t)\eta_{pcm}^{ch} \le Q_{pcm_{max}}^{ch} \tag{39}$$

$$SOC_{pcm}^{min}(t) \le SOC_{pcm}(t) \le SOC_{pcm}^{max}(t) \tag{40}$$

$$SOC_{pcm}^{0} = SOC_{pcm}^{End} \tag{41}$$

$$SOC_{bat}^{0} = SOC_{bat}^{End} \tag{42}$$

$$Q_{pcm}(t) = Q_{pcm}^{ch}(t) - Q_{pcm}^{dis}(t) \tag{43}$$

Device operation mode constraints

Because the battery and single storage hot water tank can not be charged and discharged at the same time, and the heat pump is set not to run in PV/T direct heating mode.

$$0 \le I_{bat,t}^{ch} + I_{bat,t}^{dis} \le 1 \tag{44}$$

$$0 \le I_{pcm,t}^{ch} + I_{pcm,t}^{dis} \le 1 \tag{45}$$

$$\begin{cases} I_{PV/T,t} = 1, I_{pcm,t}^{ch} = I_{hp,t} = 0 \\ I_{PV/T,t} = 0, I_{pcm,t}^{ch} = 0 \; or \; I_{hp,t} = 0 \end{cases} \tag{46}$$

4 Case study

4.1 Case parameters and scenario settings

To save computational resources as much as possible, four typical months—January, April, July, and September—are used to represent the changes in climate conditions and energy consumption throughout the year for the energy system. The Typical daily meteorological conditions, including solar radiation, wind speed, air temperature and wet-bulb temperature, is shown in Fig.2. The technical parameters of the energy storage equipment are referenced from Ref.[33], and the economic parameters of the equipment are shown in Table 1. The electricity price for selling to the grid is 0.6 yuan/kWh, and the capacity tariff is 40 yuan/month. However, the electricity price for purchasing from the grid is subject to time-of-use pricing, as shown in Table 2. The division of various scenarios is shown in Table 3.

In the subsequent scenario analysis, the research object of all scenarios is based on the heat pump microgrid model established in Chapter 2, adopting the "configuration-operation" bi-level optimization simulation method proposed in Chapter 3.

Table 1 Equipment economic and technical parameter

Equipment	Battery	SEHP	Thermal storage tank
Unit investment	1000 yuan/kWh	10000 yuan/kW	600 yuan/kW
Running expense /(yuan /kWh)	0.0018	0.026	0.001
Life expectancy/year	8	20	20
Annual interest rate/%		7.8	

Table 2 Time-sharing electricity price table

Time		Non-summer time-sharing electricity price /(YUAN /kWh)	Summer time electricity price / (YUAN /kWh)
Valley time	1:00~6:00,23:00~24:00	0.364	0.299
Usual time	7:00~8:00,12:00~18:00	0.752	0.787
Peak time	9:00~11:00,19:00~21:00	1.222	1.257

Table 3 division of different scenarios

Scenario	CHHP	SEHP	Power load DR	Tiered carbon trading
0	√	×	×	×
1	×	√	×	×
2	×	√	√	×
3	×	√	√	√

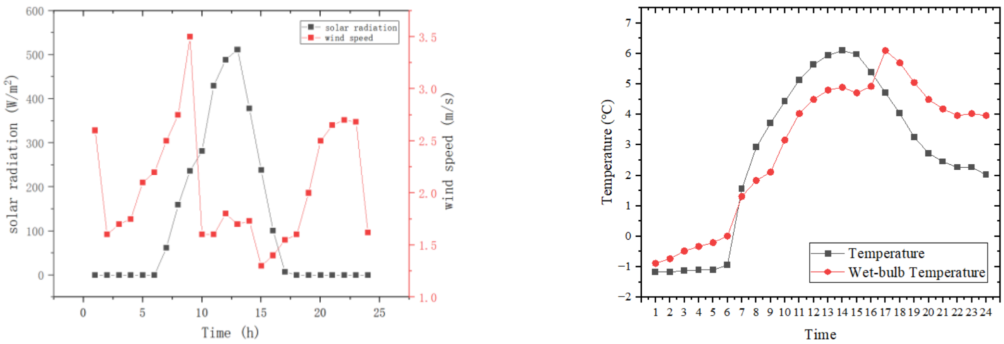

(a) Solar radiation and wind speed (b) Temperature

Fig.2 Typical daily meteorological conditions

4.2 Result and analysis

As shown in Table 4, compared with Scenario 0, Scenarios 1, 2, and 3 are additionally equipped with thermal storage tanks, enabling more energy to be stored in the form of thermal energy. When comparing Scenarios 1 and 2, it can be observed that Scenario 2 incorporates flexible thermal loads into its configuration optimization, resulting in reduced user loads and lower annual costs. Since the main load of this campus microgrid system is thermal load, the heat pump capacity in Scenario 2 is increased by 17.75%, and the capacities of the thermal storage tank and PV/T are also expanded—allowing more energy to be stored as thermal energy within the microgrid of Scenario 2. Building on Scenario 2, Scenario 3 further introduces a tiered carbon trading mechanism. Consequently, compared to Scenario 2, the battery configuration in Scenario 3 is increased by 25.68%, with slight increases in the capacities of the heat pump, PV/T, and battery. Due to the consideration of tiered carbon trading in Scenario 3, the microgrid deploys more distributed energy for heating and power generation, thereby reducing its reliance on grid electricity and minimizing carbon trading costs as much as possible. All of Scenarios 1, 2, and 3 are configured with PV/T, which not only increases distributed power generation but also reduces the consumption of electrical energy for heat production. Therefore, even though the average investment of Scenario 0 is 70.60% lower than that of Scenarios 1, 2, and 3, and the total annual expenditure of Scenario 1 is lower than that of Scenario 0, the total annual expenditure of Scenario 2 (after considering DR) is 10.95% lower than that of Scenario 1. Furthermore, in Scenario 3 with tiered carbon trading, the difference between total expenses and annual investment costs (i.e., the sum of operation and maintenance costs and electricity purchase costs) is 15.25% lower than that of Scenario 2. This indicates that DR and tiered carbon trading can stimulate the system to adopt more distributed energy configurations and reduce its consumption of electricity from the regional power grid.

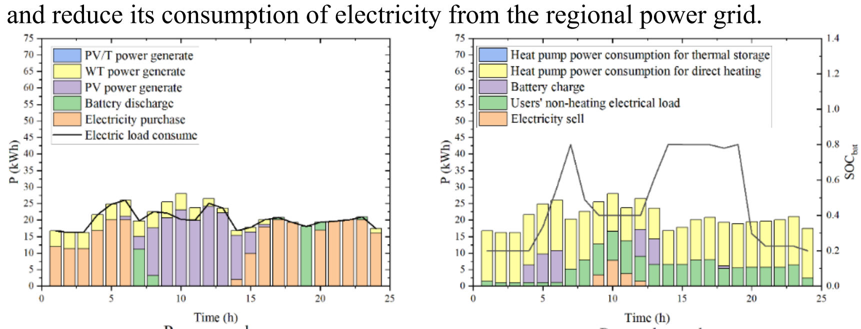

Power supply Power demand

(a) Scenario 0

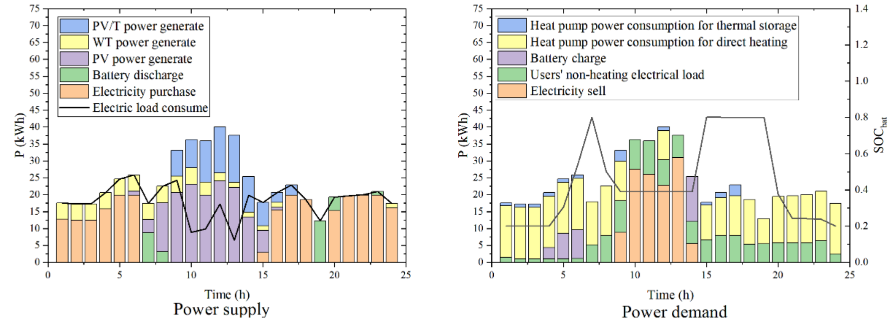

(b) Scenario 1

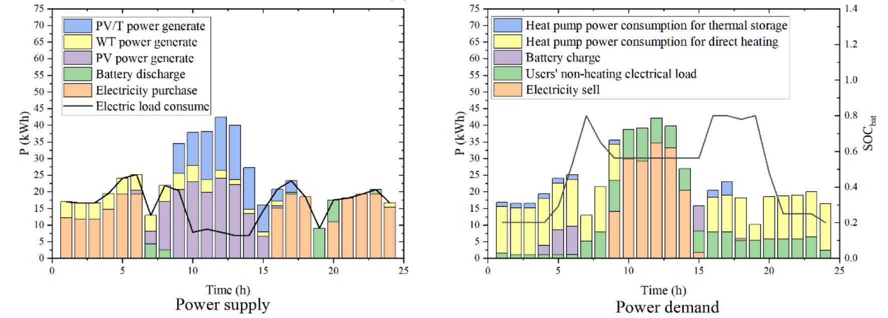

(c) Scenario 2

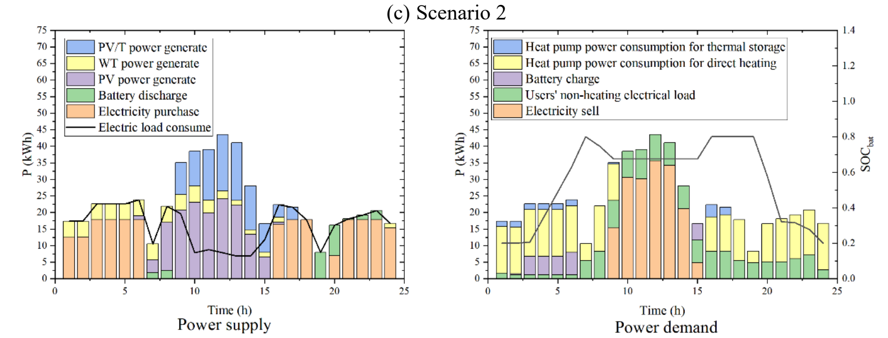

(d) Scenario 3

Fig.3 Power balance diagram

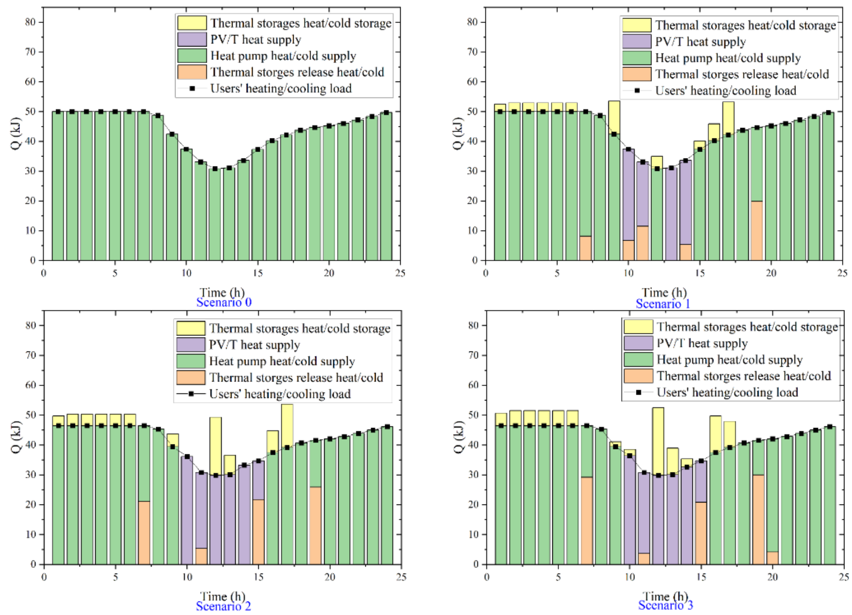

Fig.4 Thermal energy scheduling diagram

Table 4 Configuration optimization results under different scenarios

Configuration \ Scenario	0	1	2	3
Battery capacity/kW	37.64	30.65	29.94	37.63
Heat pump capacity/kW	15.15	23.55	27.73	29.51
PV/T configuration/m^2	-	214.06	252.08	268.27
Thermal storage tank capacity/kW	0	24.39	31.82	41.92
C_{inv}/yuan	17138.33	54076.62	62817.05	68360.15
C_{up}/yuan	31380.98	19603.22	17154.49	22903.31
Carbon trading price / yuan	/	/	/	5377.29

Table 5 Comparison of typical daily operation optimization results

Scenario	Typical winter electricity cost / yuan	Peak power of electricity purchase/kWh	Peak power of electricity sell/kWh	Effective penetration of renewable energy/%	Peak and valley filling coefficient	Direct solar heating ratio/%
0	168.43	20.02	7.73	40.07	89.95	0
1	94.36	19.88	30.99	42.90	274.84	10.61
2	56.10	19.28	34.60	43.39	343.96	17.05
3	44.72	17.61	35.97	45.27	352.05	17.27

As shown in Fig. 3, the electricity purchased by Scenario 0 from 14:00 to 18:00 mainly meets users' electric heating load during this period. In contrast, the electricity purchased by Scenario 1 from 15:00 to 18:00 and by Scenarios 2 and 3 from 16:00 to 18:00 not only satisfies the electric heating load but also uses thermal storage tanks for heat storage at flat electricity prices in advance to reduce the typical daily electricity cost of the microgrid. Battery discharge is concentrated at 7:00~8:00 (triggered by rising electricity prices) and 19:00~20:00 (peak electricity price period). During the noon of a typical day with large photovoltaic power output, the microgrid sells electricity to the grid after meeting users' electric heating demand. From Scenario 0 to Scenarios 1-3, with the increase in PV/T capacity configuration and the consideration of thermal elastic load, the duration of electricity sales to the grid extends. Scenario 2 incorporates electricity price demand response, expanding the peak-valley electricity price difference, and its peak-shaving and valley-filling coefficient is 25.15% higher than that of Scenario 1. Compared with Scenario 1, there is no significant increase in its peak power purchase and purchase duration, but the power sales duration increases significantly.

As shown in Fig. 4, Scenario 1 does not install thermal storage tanks due to investment costs, so the daily thermal load is fully met by direct heat pump heating. Scenarios 2 and 3 store heat during the off-peak electricity price period of 1:00~6:00, and the heat storage pauses at 7:00 due to rising electricity prices. Since this study assumes that heat pumps stop operating during PV/T direct heating, thermal storage tanks need to store more heat before PV/T direct heating is activated (before 10:00), so heat pump energy storage is performed at 9:00 in Scenarios 1, 2, and 3. Compared with Scenario 0, after adopting solar heat pumps, Scenarios 1, 2, and 3 all implement PV/T direct heating from 10:00 to 15:00. Among them, due to the increased PV/T configuration, Scenarios 2 (12:00~13:00) and 3 (12:00~14:00) can not only provide direct heating to meet the thermal load during the user response period but also store excess heat. Later, when solar radiation intensity is insufficient, the heat supply switches back to direct heat pump heating with simultaneous energy storage, and thermal storage tanks release heat at 19:00 to reduce electricity consumption for heating during peak price periods.

As presented in Table 5, Scenario 0 is not equipped with PV/T for solar thermoelectric coupling, resulting in the lowest renewable energy power penetration rate and relatively small electricity sales to the regional grid. Thus, its peak-shaving and valley-filling coefficient is 72.2% lower on average than that of Scenarios 1, 2, and 3. Compared with Scenario 1, Scenario 2 increases PV/T and heat pump configurations, raising the effective penetration of renewable energy by 8.29% and the peak-shaving and valley-filling coefficient by 25.15%. The additional PV/T and thermal storage tanks also reduce battery capacity, allowing more energy to be stored as heat, with the proportion of direct solar heating 60.7% higher than that in Scenario 1. Scenario 3 considers tiered carbon trading, reducing reliance on the regional grid. Its direct solar heating proportion is approximately 1.9% higher than that of Scenario 2, leading to lower typical daily electricity costs. This indicates that tiered carbon trading can encourage heat pump microgrids to reduce electricity purchases from the regional grid.

5 Conclusion

Through the study of a typical microgrid in urban buildings containing solar heat pumps, this paper draws the following two conclusions after the double-layer optimization of capacity and operation of the microgrid:

（1） Scenario 1 deploys a solar energy storage heat pump, which increases distributed power generation and cuts electricity costs by 37.53% relative to Scenario 0. The introduction of DR further reduces electricity costs by 12.49% and optimizes the heat pump capacity, confirming DR's positive effects on the system's economy and environmental performance. Scenario 3, with the tiered carbon trading mechanism adopted, further expands the capacities of heat pumps and batteries, lowering reliance on grid power.

（2） DR extends the microgrid's electricity sales duration to the main grid and widens the peak-valley price gap, driving a 25.15% rise in the peak-shaving and valley-filling coefficient versus Scenario 1. This improves the main grid's peak-valley adequacy and enhances the microgrid's operational flexibility.

（3） DR and tiered carbon trading promote the capacity expansion of PV/T devices. When direct heating satisfies the thermal load, excess heat can be stored, thus decreasing heating power consumption during peak-price periods.

（4） Enhanced PV/T configuration elevates the system's renewable energy penetration rate, which is further increased by 8.29% in Scenario 2 with DR applied. Scenario 3, considering tiered carbon trading, sees a 1.9% growth in direct solar heating proportion and a lower daily electricity cost, indicating that the tiered carbon trading mechanism curbs the microgrid's electricity purchase from the main grid.

Acknowledgements

This work is supported by the National Natural Science Foundation of China (52176012). Acknowledges The Energy Foundation (G-2509-36890). Acknowledges Energy Science and Technology discipline under the Shanghai Class IV Peak Disciplinary Development Program, China.

References

[1] UDDIN M, MO H, DONG D, et al. Microgrids: A review, outstanding issues and future trends[J/OL]. Energy Strategy Reviews, 2023, 49: 101127.

[2] QI J, YAN X, LIU Q, et al. Economic dispatch and flexibility enhancement of multi-energy microgrid considering cross-seasonal heat balance of ground source heat pump[J/OL]. Energy Reports, 2023, 9: 358-369.

[3] TAHERI B, JABARI F, AKBARI FOROUD A. A green cogeneration microgrid composed of water-source heat pumps, a gravity energy storage, and a bio-fueled gas turbine: Design and techno-economic optimization[J/OL]. Sustainable Cities and Society, 2023, 95: 104594.

[4] MI P, ZHANG J, GAO J, et al. Study on optimal allocation of solar photovoltaic thermal heat pump integrated energy system for domestic hot water[J/OL]. Renewable Energy, 2023, 219: 119433.

[5] LI F, XING L, SU W, et al. An idea to construct integrated energy systems of data center by combining CO2 heat pump and compressed CO2 energy storage[J/OL]. Journal of Energy Storage, 2024, 75: 109581.

[6] ZHANG Z L, ZHANG H J, XIE B, et al. Energy scheduling optimization of the integrated energy system with ground source heat pumps[J/OL]. Journal of Cleaner Production, 2022, 365: 132758.

[7] WU Z, XU G, ZHANG W, et al. Thermodynamic and economic analysis of a new methanol steam reforming system integrated with CO2 heat pump and cryogenic separation system[J/OL]. Energy, 2023, 283: 128501.

[8] Yang Z, Wang Z, Xu J, Zhao G, Ma S, Wang J. Investigation on electric heat pump solutions for carbon reduction in an integrated energy system with the coal-fired combined heat and power unit. Journal of Cleaner Production 2025,489:144705.

[9] KUMAR G M S. The positive and negative impact of novel utility demand response programme and stochastic utility-driven events on renewable penetration and flexibility activation of train and station systems[J]. Sustainable Energy, 2024.

[10] DAI M, LI H, WANG S. Event-driven demand response control of air-conditioning to enable grid-responsive buildings[J/OL]. Automation in Construction, 2023, 150: 104815.

[11] RINALDI A, YILMAZ S, PATEL M K, et al. What adds more flexibility? An energy system analysis of storage, demand-side response, heating electrification, and distribution reinforcement[J/OL]. Renewable and Sustainable Energy Reviews, 2022, 167: 112696.
[12] BORUAH D, SINGH CHANDEL S. A comprehensive analysis of eight rooftop grid-connected solar photovoltaic power plants with battery energy storage for enhanced energy security and grid resiliency[J/OL]. Solar Energy, 2023, 266: 112154.
[13] Lin Q, Lu S, Yue L, Li B, Zhu H. Research on low-carbon district heating system planning approach based on thermal energy grade and integrated demand response. Energy and Buildings 2025, 337:115660.
[14] Knudsen BR, Zotică C, Rohde D, Foslie SS, Walnum HT. Assessing demand response in district heating with waste-heat utilization. Sustainable Cities and Society 2025, 124:106270.
[15] Moradi M, Farzaneh H. Demand response programs in decentralized hybrid local energy markets: evaluating the impact of risk-adjusted behavior of market players and the integration of renewable energy sources, using a novel bi-level optimization framework. Applied Energy 2025;390:125806.
[16] Li R, Tu Q, Feng H, Zou Z. Demand response based battery energy storage systems design and operation optimization. Energy and Buildings 2025, 338:115738.
[17] Jikai Wang, Qunzhi ZhuCA1, Jingyong Cai, et al. Design and experimental study of a novel flexible PV/T structure[J]. Energy,2024, Vol.296: 131139.
[18] VAHIDHOSSEINI S M, RASHIDI S, HSU S H, et al. Integration of solar thermal collectors and heat pumps with thermal energy storage systems for building energy demand reduction: A comprehensive review[J/OL]. Journal of Energy Storage, 2024, 95: 112568.
[19] Mulleriyawage UGK, Shen WX. Optimally sizing of battery energy storage capacity by operational optimization of residential PV-Battery systems: An Australian household case study. Renewable Energy 2020, 160:852–64.
[20] Modu B. Operational strategy and capacity optimization of standalone solar-wind-biomass-fuel cell energy system using hybrid LF-SSA algorithms. International journal of hydrogen energy n.d.
[21] Yang H. Operation strategy and optimization configuration of hybrid energy storage system for enhancing cycle life. Journal of Energy Storage 2024.
[22] Kang J, Wang J, Liu C, Ye S, Yang M. Coordinated optimization of configuration and operation of a photovoltaic integrated building cooling system with electricity and ice storages under source-load uncertainties. Energy and Buildings 2024, 320:114600.
[23] https://iea-pvps.org/wp-content/uploads/2021/07/Report-IEA%E2%80%93PVPS-T13-16_2021_Service_Life_Estimation_4_PV_Modules.pdf.
[24] Weiß K-A, Klimm E, Kaaya I. Accelerated aging tests vs field performance of PV modules. Prog Energy 2022, 4:42009.
[25] Kirchem D, Dereli RK, Lynch MÁ, Casey E. Demand response within the irish wastewater treatment sector: analysing flexibility potentials of the aeration process and wastewater pumping within an integrated energy–water system model. Appl Energy 2025, 381:125128.
[26] Mo, Qiu, Liu, et al. Modeling and optimization for distributed microgrid based on Modelica language[J]. APPLIED ENERGY,2020,Vol.279: 115766.
[27] MALEHMIRCHEGINI L, FARZANEH H. Demand response modeling in a day-ahead wholesale electricity market in Japan, considering the impact of customer risk aversion and dynamic price elasticity of demand[J/OL]. Energy Reports, 2022, 8: 11910-11926.
[28] Chen C Y, Hu B, Xie K G, et al. Time-of-use pricing model considering power system reliability and electricity purchasing risk[J]. Power System Technology, 2014, (8): 2141-2148.
[29] Wei Z B, Ma X R, Guo Y, et al. Optimal operation of integrated energy system considering demand response under carbon trading mechanism[J]. Electric Power Construction, 2022, 43(1): 1-9.
[30] WANG Y, LI Y, ZHANG Y, et al. Optimized operation of integrated energy systems accounting for synergistic electricity and heat demand response under heat load flexibility[J/OL]. Applied Thermal Engineering, 2024, 243: 122640.
[31] FAN H, YUAN Q, CHENG H. Multi-objective stochastic optimal operation of agrid-connected microgrid considering an energy storage system[J]. Applied Sciences-Basel,2018, 8(12): 2560.
[32] Xu R, Liu F. Dynamic modeling and co-optimization of configuration and operation for a solar-assisted ejector heat pump with energy storages. Energy 2025, 320:135094.
[33] Yu, Yan,Liu,et al. Optimization of integrated energy system with phase-change energy storage heat pump considering thermal inertia[C]//18th IBPSA Conference on Building Simulation, BS 2023. 2023.